Case Studies in Thermal Engineering 25 (2021) 100952

Contents lists available at ScienceDirect

Case Studies in Thermal Engineering

journal homepage: http://www.elsevier.com/locate/csite

Transient conjugate natural convection heat transfer in a differentially-heated square cavity with a partition of finite thickness and thermal conductivity

Mehdi Khatamifar *, Wenxian Lin, Liqiang Dong

College of Science & Engineering, James Cook University, Townsville, QLD 4811, Australia

ARTICLE INFO

Keywords:
Unsteady conjugate natural convection
Heat transfer
Partition
Thermal conductivity

ABSTRACT

The transient conjugate natural convection heat transfer in a differentially-heated cavity with a partition of finite thickness and thermal conductivity are investigated numerically over the range of the Rayleigh number from 10^3 to 10^8, the thermal conductivity ratio of partition to that of fluid from 0.1 to 1000, and the dimensionless partition thickness from 0.05 to 0.2. An analysis of the obtained temperature contours and profiles, the time for the onset of stratification and the Nusselt number shows that the thermal conductivity ratio effect is significant only over the range of 0.1–10, when the role played by the partition changes, whereas the effect becomes negligible as the thermal conductivity ratio is very large (100 or beyond). It is also found that the scaling relations developed for the non-partitioned cavity are found to be applicable for the partitioned cavity. The results further show that the effect of the partition thickness on heat transfer is significant mainly when the thermal conductivity ratio is small.

1. Introduction

This work is focused on the transient behaviour of conjugate natural convection heat transfer in a differentially-heated, partitioned square cavity with the partition of finite thickness and thermal conductivity. It is a continuation of our previous study [1] which focused on the steady-state situation of the problem.

Transient natural convection flow and heat transfer occur in many applications such as heat exchangers, energy transfer in rooms and buildings, cooling of electronic equipment, solar collectors, etc. [2–10]. Hence, understanding the transient development, flow structure, and heat transfer in such a flow is of significance and has attracted extensive research interest. In particular, the unsteady, transient natural convection flow and heat transfer in a cavity with differentially-heated side walls has been widely studied under a variety of configurations (see, *e.g.* Refs. [11–15]), subject to various constant and time-varying heating/cooling conditions (see, *e.g.* Refs. [16–20]). A combination of analytical (such as scaling analysis), numerical and experimental methods have been used to explore the behaviour of such flows (see, *e.g.* Refs. [21–24]).

Many applications involve unsteady, transient conjugate natural convection heat transfer, which may be modelled by a differentially-heated cavity, in which a vertical heat-conducting partition with a finite thickness divides the cavity into two separate enclosures, with the flows within these two enclosures coupled through the partition via heat conduction [25,26]. Inspired by the oil tank cooling process in a wrecked ship immersed in the sea, Xu et al. [22] numerically investigated the transient behaviour of the

* Corresponding author.
E-mail address: mehdi.khatamifar2@jcu.edu.au (M. Khatamifar).

https://doi.org/10.1016/j.csite.2021.100952
Received 18 January 2021; Received in revised form 15 March 2021; Accepted 15 March 2021
Available online 26 March 2021

coupled thermal boundary layers in a differentially heated partitioned cavity filled with water. They assumed that the partition has zero thickness and identified three main stages, i.e., initial, transient and steady stage for the development of the conjugated natural convection flow. This study was expanded to investigate the coupled thermal boundary layers induced by a fin attached to the partition [27]. Williamson, Armfield and Kirkpatrick [28] numerically studied the transient behaviour of differentially heated partitioned cavity for $0.6 \times 10^{10} \leq Ra \leq 1.6 \times 10^{10}$ and the aspect ratio of 1–2. The partition they considered was vertical and at the center of the cavity with infinite conductivity. It was reported that at the fully developed stage, the transition to chaotic flow is caused by the instability of the convective boundary layer and the perturbations in the thermal boundary layers of the partition sides can affect each other through the partition.

The presence of two or more sub-domains separated by heat conducting partition(s) in con-jugate heat transfer problems arouses considerable interest in analytical studies. Viskanta and Abrams [29] obtained an exact solution of the temperature distribution for laminar conjugate natural convection in the case of constant properties, concurrent and inviscid flow. They re-ported for the first time that the omission of thermal interaction between both sides of the partition can result in large inaccuracy. This finding encouraged further early analytical studies on this topic [30–32].

Due to the major influence of the heat-conducting partition on the flow behaviour and heat transfer in a cavity, different parameters of the partition such as its position, thickness, thermal conductivity, shape, and angle have been extensively investigated. Ghosh et al. [33] studied the effect of the partition position on the flow field and heat transfer in a partitioned cavity and reported that the partition location does not have a significant effect on the heat transfer when the Rayleigh number (Ra) is in the range of 10^3 to 10^7. The effect of the position of a partition with very high thermal conductivity was studied by Tong and Gerner [34] in an air-filled rect-angular enclosure. For $10^4 \leq Ra \leq 10^5$, they found that a centrally positioned partition results in the largest reduction in heat transfer. More realistic assumptions on the thermal conductive partitions were used by Kahveci [35] who examined the effect of the thickness, conductivity, and position of the partition on the steady-state Nusselt number over $10^4 \leq Ra \leq 10^6$ and reported that the average Nusselt number decreases asymptotically when the partition position changes from the left wall to the center of the cavity and the partition thickness has an insignificant effect on the thermal behaviour of the partitioned cavity, whereas the effect of the partition thermal conductivity is substantial. This observation was also reported by Kangni et al. [36], who investigated the heat transfer in a tall cavity with a vertical heat conductive partition. Khatamifar et al. [1] investigated the effects of the thickness and position of a heat conducting partition with finite thermal conductivity and thickness on the average Nusselt number over $10^5 \leq Ra \leq 10^9$ and reported that the Nusselt number decreases when the partition thickness increases, but the effect of the partition position is negligible. The aspect ratio has also been reported to affect the heat transfer in a partitioned cavity. Kahveci [37] reported that an in-crease in the

Table 1
Some of the leading studies on the conjugate natural convection [1,22,33–37,39,40,42–48].

Authors	Ra	Pr	Number of partitions	A
Williamson and Armfield [42]	0.6×10^{10}– 1.6×10^{10}	7.5	1	2
Xu *et al.* [22]	9.2×10^8	6.63	1	1
Saha *et al.* [43]	$10^3 - 10^9$	0.71	1	1
Acharya and Tsang [44]	up to 10^7	0.71	1	$1 - 2$
Turkoglu and Yucel [45]	$10^5 - 10^7$	0.71	$0 - 4$	$0.5 - 1.5$
Cuckovic-Dzodzo *et al.* [40]	$10^4 - 10^6$	$2700 - 7000$	$0 - 1$	1
Nishimura *et al.* [39]	$10^8 - 10^{10}$	6	$0 - 4$	4
Ghosh *et al.* [33]	$10^3 - 10^6$	1	1	1, 0.8, 0.5 and 0.4
Tong and Gerner [34]	$10^4 - 10^5$	0.71	1	5, 7.5, 10, 12.5 and 15
Kahveci [35]	$10^4 - 10^6$	0.71	1	1
Khatamifar [1]	$10^5 - 10^9$	0.71	1	1
Kangni *et al.* [36]	$10^3 - 10^7$	0.72	$1 - 5$	$5 - 20$
Kahveci [37]	$10^4 - 10^6$	0.71	1	$0.25 - 4$
Hanjalić *et al.* [46]	$10^{10} - 10^{12}$	air & water	$0 - 1$	0.5, 0.33 and 0.66
Nansteel and Greif [47]	$10^{10} - 10^{11}$	$3.5 - 7$	$0 - 1$	0.5
Xu *et al.* [48]	$10^9 - 10^{11}$	7.8	1	1

aspect ratio results in heat transfer enhancement. Overall, the previous studies on the laminar natural convection flow show that the presence of a partition, even with infinite thermal conductivity, reduces natural convection heat transfer in comparison with that in a non-partitioned enclosure and the scaling law of $Nu \sim Ra^{1/4}$ is obtained [1,35,38–41]. Table 1 presents some of the leading studies on the conjugate natural convection in a partitioned cavity. From the previous studies, it can be seen that the focus has been only on very thin partitions (*e.g.* Refs. [27,49,50]) or partitions with infinite thermal conductivity (*e.g.* Ref. [28]), even for some quite recent studies. It was also reported that ignoring or oversimplifying the coupling between both sides of the conducting partition can cause substantial inaccuracy [29].

The present study is motivated by the poor understanding of the transient conjugate natural convection flow and heat transfer in a differentially-heated cavity with a partition which is of finite thickness and thermal conductivity.

2. Numerical methodology

The details of the numerical methodology used in this paper are provided in the Supplementary Materials part. Some of these details were also presented in Ref. [1]. Only the most specific details about the numerical methodology used in this study are described below.

The physical domain of this study is a two-dimensional partitioned rectangular cavity with height H and width L with the aspect ratio of $A = H/L$. The domain in non-dimensional form is illustrated in Fig. S1 in the Supplementary Materials. The sidewalls are isothermal fixed at T_h and T_c, respectively ($T_h > T_c$), with the dimensionless temperatures $\theta = 1.0$ and $\theta = 0.0$, respectively, where temperature is made dimensionless by $\theta = (T - T_c)/(T_h - T_c)$, and the top and bottom walls of the cavity are insulated. A partition with the dimensionless thickness T_p is placed with its middle at the dimensionless location X_p from the left wall, where both T_p and X_p are made dimensionless by L. The working fluid is air with the Prandtl number of $Pr = 0.71$, which is initially quiescent and at a temperature of $(T_h + T_c)/2$, *i.e.*, at $\theta = 0.5$. All walls and the partition are assumed to be rigid and no-slip. The partition is thermally conductive, with finite thermal conductivity of k_s.

The flow and heat transfer within a partitioned square cavity (*i.e.*, $A = 1$) are governed by Ra, Pr, T_p, X_p, and the thermal conductivity ratio of fluid and partition wall k_r, with Ra, Pr and k_r are defined as follows,

$$Pr = \frac{\nu_f}{\alpha_f}, Ra = \frac{g\beta_f(T_h - T_c)H^3}{\nu_f \alpha_f}, k_r = \frac{k_s}{k_f} \tag{1}$$

in which g is the acceleration due to gravity, ν_f, α_f, β_f and k_f are the kinematic viscosity, thermal diffusivity, coefficient of volumetric expansion and thermal conductivity of the fluid, respectively.

The governing equations are two-dimensional incompressible Navier-Stokes and tempera-ture equations with the Boussinesq approximation for buoyancy. They were discretized using the finite volume method and solved by the SIMPLE algorithm. For the advection, the time integration and the rest of terms, the QUICK scheme, the Adams-Bashforth scheme and the second-order central difference scheme were employed, respectively. A non-uniform rectangular mesh was generated. The areas close to the walls and the partition have finer grids than the core regions. The initial and boundary conditions as well as the benchmark against the available results are presented in the Supplementary Materials.

To ensure the obtained numerical solutions be grid independent, a study was carried out with four meshes (100×100, 150×150, 250×250, 300×300) for the case of $T_p = 0.2$, $X_p = 0.5$, $k_r = 1000$, $Pr = 0.71$ and $Ra = 10^8$ with a convergence criterion of 10^6 for all residuals. The obtained time series of the average Nusselt number on the hot wall with these meshes are presented in Fig. S2 in the Supplementary Materials. Since the variation of results between the 250×250 mesh and the 300×300 mesh is less than 2% for the average Nusselt number and less than 1% for temperature, the 250×250 mesh is selected as the mesh for all numerical simulations in this study. The smallest and largest grid sizes of the mesh are 0.000807 and 0.007256, 0.000806 and 0.007255 in the x and y

Table 2
Comparison between the average Nusselt number obtained from the present study and those available in the literature for a differentially heated square cavity at various Rayleigh values.

	$Ra = 10^3$	$Ra = 10^4$	$Ra = 10^5$	$Ra = 10^6$	$Ra = 10^7$	$Ra = 10^8$
This study	1.117	2.244	4.521	8.825	16.528	30.245
[52] (experimental)	–	1.246	3.916	7.883	15.38	31.22
[53]	1.117	2.243	4.519	8.820	16.504	–
[54]	1.118	2.244	4.520	8.822	16.82	–
[55]	1.121	2.244	4.520	8.822	16.79	30.506
[56]	1.118	2.286	4.546	8.652	–	–
[57]	1.118	2.243	4.519	8.799	–	–
[58]	1.1178	2.245	4.522	8.825	16.52	–
[59]	–	–	–	–	16.523	30.225
[60]	–	–	4.521	8.825	16.523	–
[61] (Fluent)	1.113	2.246	4.535	8.861	16.645	28.52
[61] (OpenFOAM)	1.109	2.222	4.498	8.786	16.502	30.1425
[62]	1.074	2.084	4.3	8.743	13.99	–
[51] (FEM)	1.117	2.254	4.598	8.976	16.656	31.486
[51] (DSC)	1.073	2.155	4.352	8.632	13.86	23.67

directions, respectively, and the maximum grid expansion ratio (or stretching factor) is 1.0697.

Similarly, to test the time step independence of the numerical simulations, a study was also carried out with three time steps of $d\tau = 10^{-2}$, 5×10^{-3} and 10^{-3} using the 250×250 mesh for the case of $T_P = 0.2$, $X_P = 0.5$, $k_r = 1000$, $Pr = 0.71$ and $Ra = 10^8$. The results are presented in Fig. S3 in the Supplementary Materials. It was found that the variation of results between the selected time steps are negligible, therefore, the time step of $d\tau = 5 \times 10^{-3}$ was chosen for the numerical simulations.

Moreover, the obtained average Nusslet number from this study was compared with several numerical and experimental studies, as shown in Table 2. It is seen that the results of the present study agree well with those reported in the literature up to $Ra = 10^6$; however, for higher Ra values, there is a discrepancy with some of the presented data in the literature (*e.g.* Ref. [51]). Nevertheless, in terms of the experimental results (*i.e.* [52]), the higher Ra cases show well agreement with the numerical ones, but a discrepancy at lower Ra cases found. This outcome is expected as lower Ra cases are more sensitive to the experiment errors.

The accuracy of the code was also validated for the case of a partitioned cavity. The average Nusselt number obtained for $10^4 \leq Ra \leq 10^6$ and $k_r = 1$ and 100 is presented in Table 3.

3. Results and discussion

3.1. Transient flow development

The transient development of the natural convection flow in a partitioned cavity is demonstrated in this section for different values of Ra (10^3, 10^4, 10^5, 10^6, 10^7 and 10^8), k_r (0.1, 1, 10, 100, 500 and 1000), and T_p (0.05, 0.1, and 0.2), all with $X_P = 0.5$, $H/L = 1$, and $Pr = 0.71$.

The thermal conductivity ratio selected for this work covers a wide range of materials with different applications in the industry. $k_r \approx 0.1$ represents a range of super insulating materials such as fiber fillings or powder filled panels [63]. By selecting $k_r \approx 1$, the partition represents the thermal behaviour of materials such as polyurethane foam, extruded polystyrene, some gases such as nitrogen, oxygen, water vapor, redwood bark or silica aerogel. For instance, silica aerogels have a wide range of use, mostly in high-tech science and engineering. Some of the current applications include insulation on the Mars exploration rovers, hypervelocity particle capture in the stardust probe, high-energy Cherenkov radiation particle counters, remediating oil from water, and transparent window insulation [64]. Granite, sandstone, ice, fused silica, thorium dioxide and zirconium dioxide are some of the materials that have $k_r \approx 100$. Aluminum oxide and stainless steel have $k_r \approx 500$ and beryllium oxide (a well known electrical insulator), bronze, titanium, monel, constantan, solder have $k_r \approx 1000$.

Fig. 1 presents the snapshots of temperature contours at five time instants ($\tau = 5$, 10, 50, 100 and 300) for the case of $k_r = 500$ and $T_p = 0.05$ over the course of the flow development for the left half-cavity. Due to symmetry (a 180° rotational symmetry), the results for the right half-cavity are the same as that for the left one and are therefore not presented in the figures. The results show that at the early stage, a rising natural convection boundary layer (NCBL) forms on the sidewall of the left half-cavity. At the smallest Ra value considered (*i.e.*, $Ra = 10^3$), it is seen that the temperature contours at all five time instants are almost vertical and evenly spaced across the half-cavity, indicating that pure conduction is the only mechanism for the flow and heat transfer. When Ra increases the temperature contours gradually depart from vertical ones in the core of the half-cavity, with the extent of this effect increasing with Ra. This indicates that the conduction domination gradually decreases and convection becomes dominant.

In association with this process a reduction of the NCBL thickness on the sidewall is observed, similar to the case without a partition (see, *e.g.* Ref. [12]). The stream function contours show that the flow structure also becomes more complex, departing from the simple single symmetric cell to have a distorted multi-cell appearance, as shown in Fig. S4 in the Supplementary Materials. When $Ra \geq 10^5$, the boundary layer discharges heated fluid, as an intrusion, below the top boundary, as clearly seen from the temperature contours at $\tau = 5$. The hot intrusion takes a longer time to discharge from the boundary layer to reach the partition when Ra increases. This is similar to that in a non-partitioned cavity [65], where it was found that the time for the intrusion to reach the opposite sidewall is proportional to $Ra^{\frac{1}{16}}$. After reaching the partition, the intrusion starts to mix with the fluid in the remaining region of the half-cavity, which is at the initial temperature of $\theta = 0.5$, and the filling process begins. The rate of filling reduces when Ra increases due to the thinner boundary layer on the left sidewall and thus the resulted thinner intrusion, which is again similar to that in the non-partitioned case [66]. The flows at higher Ra values are observed to be considerably more active with a more complex spatial structure during the development than that at lower Ra values, as expected.

Table 3
Comparison between the average Nusselt number obtained from the presented study and those available in the literature for a differentially heated partitioned cavity at various Rayleigh values.

$k_r = 1$	$Ra = 10^4$	$Ra = 10^5$	$Ra = 10^6$
This study	1.09	1.76	2.82
[53]	1.05	1.74	2.79
[35]	1.06	1.79	2.8
$k_r = 100$	$Ra = 10^4$	$Ra = 10^5$	$Ra = 10^6$
This study	1.17	2.11	4.03
[53]	1.05	1.87	3.51
[35]	1.19	2.14	3.93

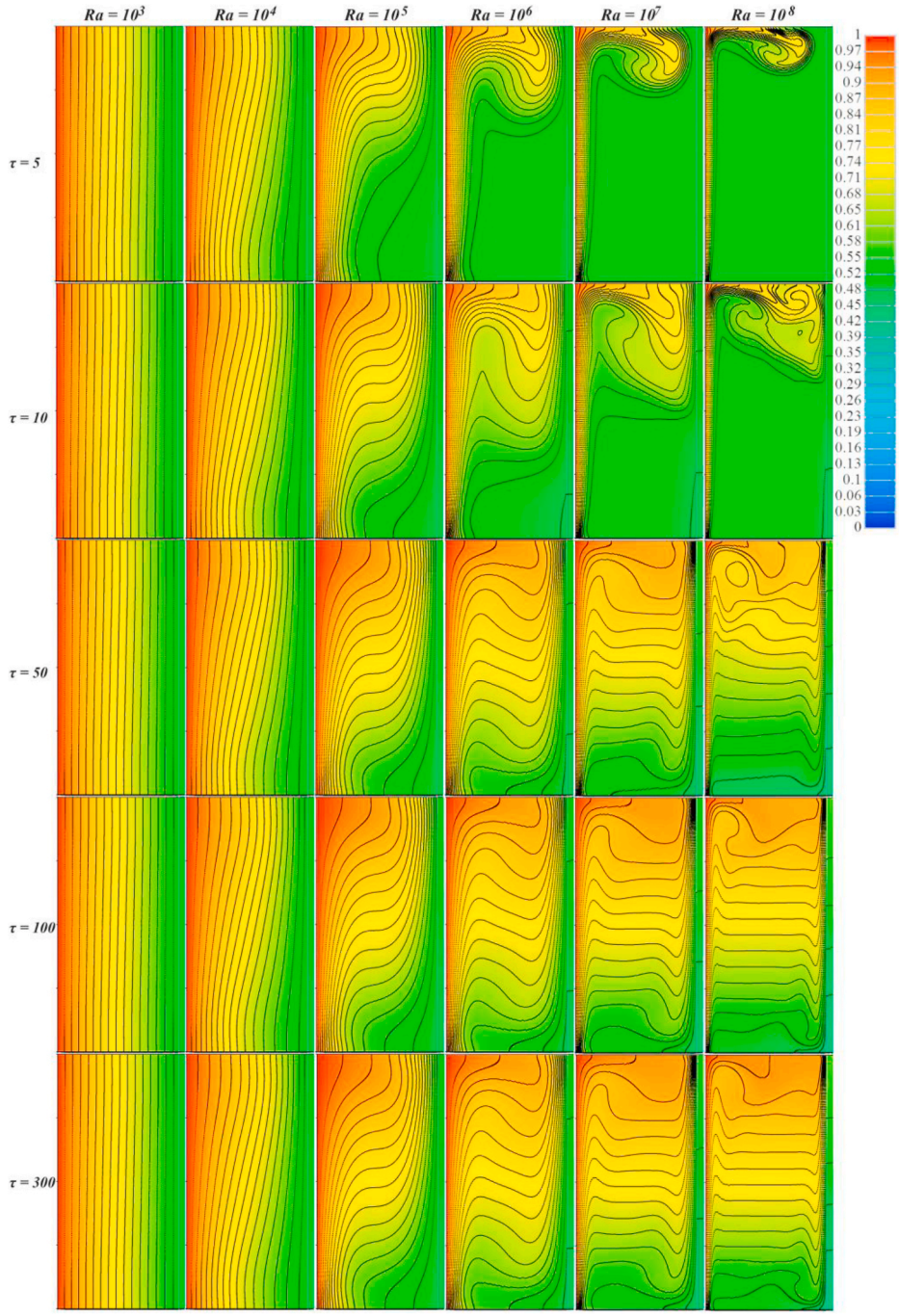

Fig. 1. Temperature contours in the left half-cavity at different times for the case of $k_r = 500$ and $T_p = 0.05$.

At long enough times, due to the combined process of the impingement of the hot intrusion on the top area of the left surface of the partition and the associated filling of hotter fluid in the left half-cavity, and the simultaneous impingement of the cold intrusion on the bottom area of the right surface of the partition and the associated filling of colder fluid in the right half-cavity, a temperature difference exists across the partition, which results in heat transfer from the left half-cavity to the right one and the flows within both half cavities become coupled, leading to conjugate natural convection boundary layers (CNCBLs) falling/rising on the left/right surface of the partition. This coupling of the heat transfer speeds up the stratification establishment within each half-cavity, due to the enhanced heat transfer rate across the partition with such a very large k_r value, when compared to the case without partition for $Ra \geq 10^5$. For smaller Ra cases, as noted above, the heat transfer is conduction dominated and there is relatively little stratification within the cavity. For $Ra \geq 10^5$, this stratification process is largely complete at $\tau = 300$ for $k_r = 500$, with a stable stratification spanning the full height

of each half-cavity and the CNCBLs on either side of the partition well established, and the flow is then at its fully developed, steady state. The results also show that the time to reach the steady state increases as Ra increases.

When k_r increases, it was found that the flow and temperature contours do not change before the intrusion to reach the partition, as expected, as there is no effect from the partition. Nevertheless, with the impingement of the hot intrusion on the left surface of the partition, the effect of partition conductivity on the flow and temperature pattern becomes significant. It is further found that the low k_r case has a hotter half-cavity compared to the higher k_r case, as shown in Figs. S5 and S6 for the case of $k_r = 0.1$ and $T_p = 0.05$ in the Supplementary Materials. This observation can be explained by the fact that the partition with low thermal conductivity provides substantial resistance to the heat transfer between the two half cavities, contrary to the high thermal conductivity case, which results in hotter and colder left and right half-cavity, respectively. This produces a significant difference in temperature variation in the half cavities and a much longer time for the filling process and the stratification establishment.

To further study the effect of k_r, the steady-state temperature contours of the cases with different k_r, all with $T_p = 0.05$, $X_p = 0.5$ and $Ra = 10^8$, are presented in Fig. 2. For $k_r = 0.1$, the isotherms in the partition are almost vertical, particularly at small Ra values, showing high thermal resistance of the partition which leads to trapping all the heated and cooled fluids on the left and right half-cavities respectively due to poor heat transfer across the partition, as can be seen in Fig. 2(a). As a result, the main temperature gradient happens across the partition and this character can be identified by the presence of the high density of the isotherms in the partition. When $k_r = 1$, as the thermal conductivity of the partition is the same as that of the fluid, the partition does not reduce or enhance the heat transfer between the two half-cavities, leading to the density of the isotherms in the partition is still high, but significantly smaller than the $k_r = 0.1$ case. By increasing k_r to 10, the partition enhances, instead of reduces, the heat transfer between the two half-cavities, which speeds up and strengthens the stratification process, leading to a reduced temperature gradient range in the half-cavity. Therefore, the number of isotherms in the partition reduces, from 22 (the total number of isotherms is 32 and 10 isotherms present in the cavity) in Fig. 2(a) for $k_r = 0.1$ to 16 in Fig. 2(c) for $k_r = 10$. This trend can be seen for the rest of the selected k_r cases as the number of isotherms in the partition decreases to 10, 4 and 2 for $k_r = 100$ (Fig. 2(d)), $k_r = 500$ (Fig. 2(e)) and $k_r = 1000$ (Fig. 2(f)), respectively. Consequently, the partition with the highest thermal conductivity (Fig. 2(f)), due to the presence of only two isotherms in the partition, can be considered to have almost constant temperature of $\theta \approx 0.5$. In addition, the angle of isotherms also reveals the characteristics of the heat transfer due to the presence of the partition. The highest thermal resistance partition ($k_r = 0.1$) shows the characteristics of an adiabatic wall with the presence of almost vertical isotherms. As thermal conductivity increases, the slope and density of isotherms decrease, with the cavity with $k_r = 1000$ showing almost horizontal isotherms in the partition which can be considered as an isotherm wall.

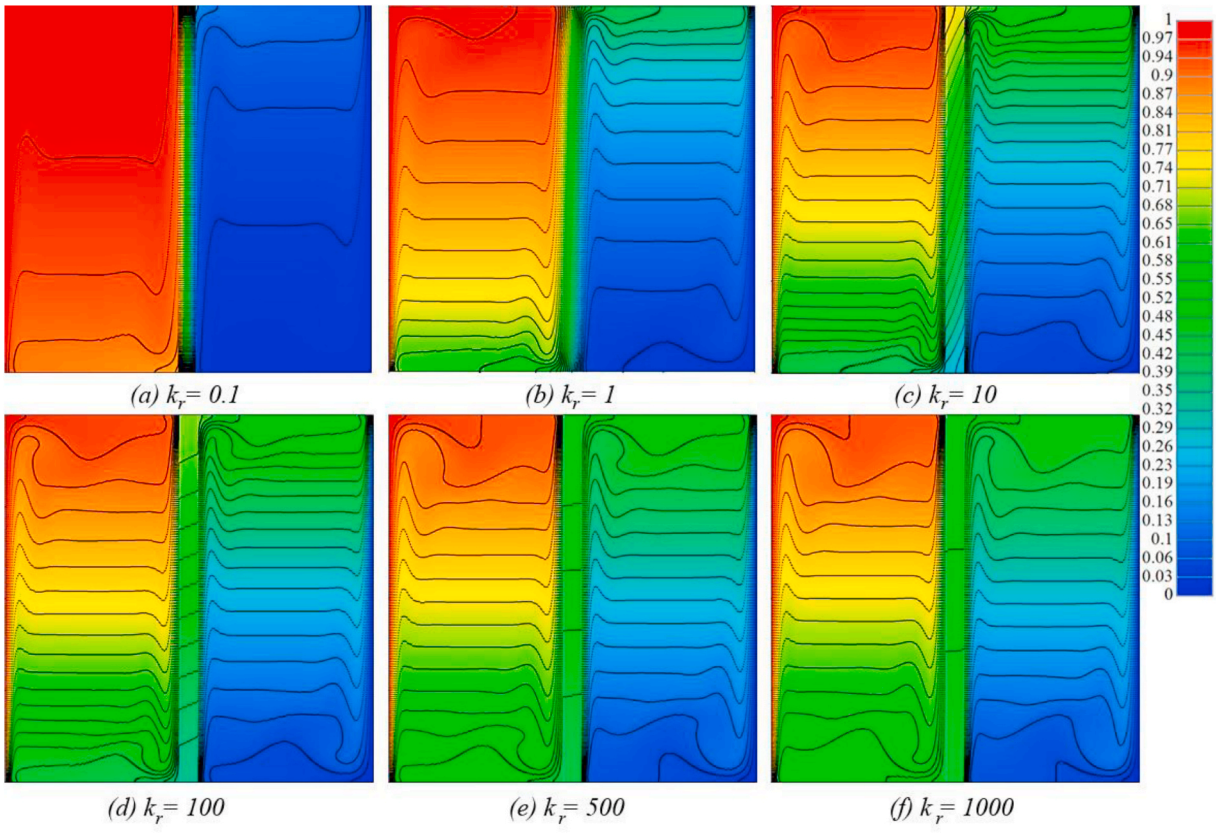

Fig. 2. Temperature contours for the cases of $T_p = 0.05$, $X_p = 0.5$ and $Ra = 10^8$ with different k_r values.

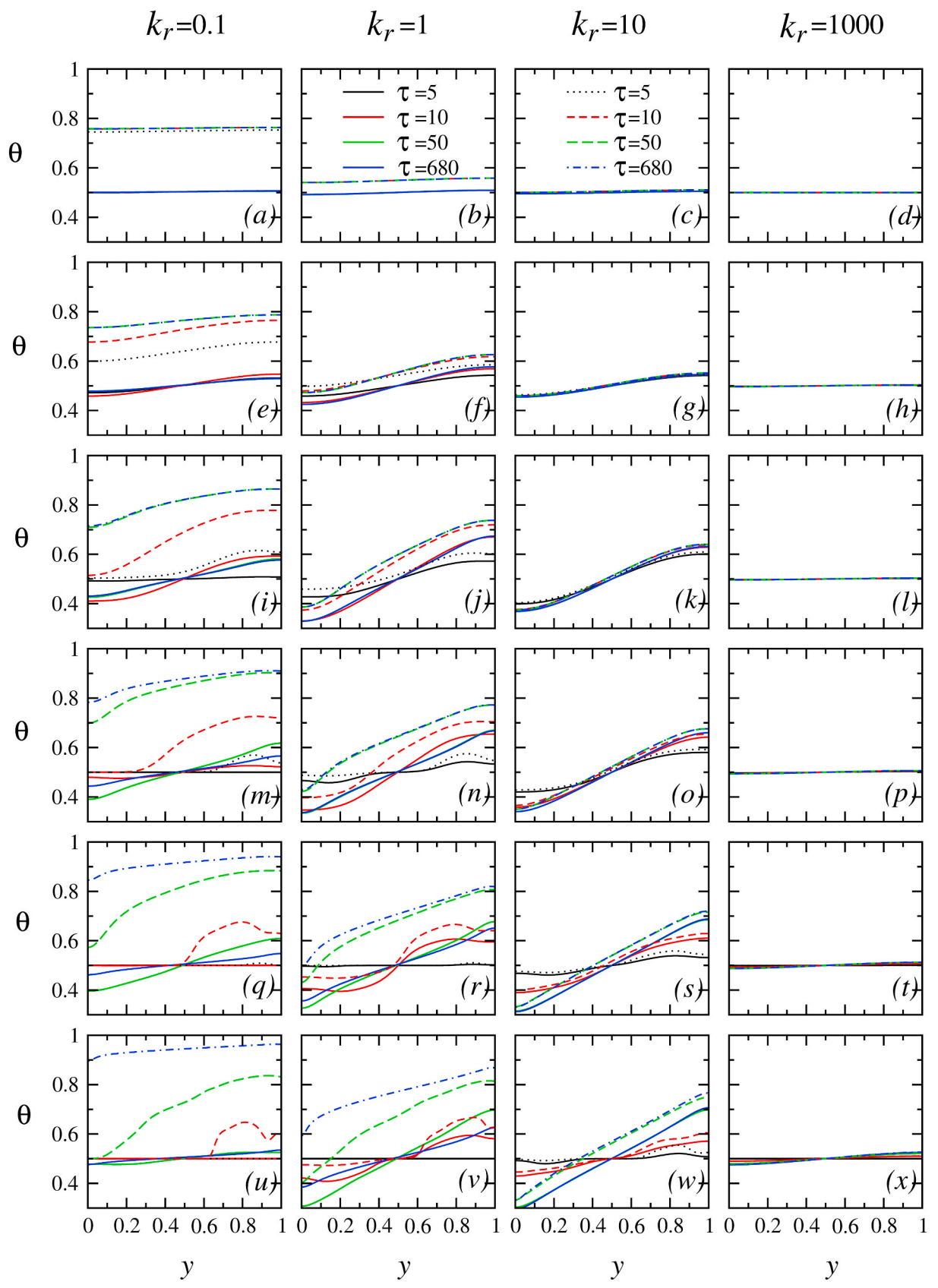

(caption on next page)

Fig. 3. The vertical temperature profiles at the middle of the partition ($x = 0.5$, solid lines) and on the left surface of the partition ($x = 0.45$, non-solid lines) at $\tau = 5$, 10, 50, and 680 for different Ra and k_r values, all at $T_p = 0.1$: (*a*)–(*d*) (first row) $Ra = 10^3$, (*e*)–(*h*) (second row) $Ra = 10^4$, (*i*)–(*l*) (third row) $Ra = 10^5$, (*m*)–(*p*) (fourth row) $Ra = 10^6$, (*q*)–(*t*) (fifth row) $Ra = 10^7$, and (*u*)–(*x*) (sixth row) $Ra = 10^8$.

As the effect of k_r on flow and heat transfer is found to be significant, as a consequence, it is expected that partition thickness T_p has an important role as well. This effect was investigated with the temperature contours for the cases with different k_r values, all with $T_p = 0.2$, $X_p = 0.5$ and $Ra = 10^8$, as shown in Fig. S7 in the Supplementary Materials. It was found that at $k_r = 0.1$, similar to the $T_p = 0.05$ case as shown in Fig. 2(*a*), the isotherms in the partition are almost vertical, showing high thermal resistance of the partition which isolates all the heated and cooled fluids on the left and right half-cavities. However, this insulating behaviour is more significant than the $T_p = 0.05$ case, as only two isotherms present in the half-cavity and the rest of 28 isotherms are in the partition. By increasing k_r to 100, on the contrary, the thermal resistance is replaced by thermal enhancement. Comparing Fig. 2(*b*) and Fig. S7(*b*), it also found that the density of isotherms and the temperature gradient range in the thicker partition are smaller than those in the thinner one. This trend was found for the rest of the selected k_r cases as the number of isotherms decreases to 16, 6, 2 and 2 for $k_r = 10$ (Fig. S7(c)), $k_r = 100$ (Fig. S7(d)), $k_r = 500$ (Fig. S7(e)), and $k_r = 1000$ (Fig. S7(f)), respectively. Consequently, the partition with the highest thermal conductivity, due to almost no presence of isotherms (as the two isotherms shown in the figure for $k_r = 1000$ are very close to the edges of the partition), can be considered as an isotherm wall, similar to the $T_p = 0.05$ case, as discussed above.

Fig. 3 presents the vertical temperature profiles at the middle of the partition ($x = 0.5$) and on the left surface of the partition ($x = 0.45$) at four time instants for different Ra and k_r values, all at $T_p = 0.1$. The vertical temperature profiles at the middle of the left half-cavity ($x = 0.225$) are shown in Fig. S8 in the Supplementary Materials. The pure conduction nature for $Ra = 10^3$ is evidently shown in the figures as all profiles are essentially vertical. For such low Ra cases, the effect of k_r observed above is clearly confirmed, as temperatures at the middle of the left half-cavity and on the left surface of the partition gradually decrease when k_r increases from $k_r = 0.1$ to $k_r = 10$ due to the improvement of heat transfer across the partition. Beyond $k_r = 10$, the profiles are essentially the same, indicating that the effect of the partition becomes negligible when k_r is very large. At the middle of the partition, all profiles are almost the same and vertical, at the value of $\theta = 0.5$, a further evidence to suggest that the heat transfer is due to pure conduction. When Ra is increased to 10^4, as shown in Fig. 3(*e*)–(*h*) and Fig. S8(*e*)-(*h*), all temperature profiles (except that for $k_r = 1000$) are not vertical anymore, indicating that convection makes a contribution to the heat transfer. However, the slopes of the profiles are small, which implies weak stratification of fluid in the left half-cavity, showing that the contribution from convection to the heat transfer is small and conduction is still the predominant heat transfer mechanism. The effect of k_r is seen to be basically similar to that observed above for the $Ra = 10^3$ cases, although with a few noticeable differences. When k_r is very small ($k_r = 0.1$), the slopes of the profiles are very small, particularly at the steady states. With the increase of k_r, in particular for $k_r > 1$, the slopes increase due to the enhanced heat transfer between the two half-cavities and are almost linear in the half-cavity, which indicates a strengthened stratification, except at the top and bottom regions. At the top region, the temperature is essentially the same due to the intrusion which makes the fluid within this small region well mixed. This occurs similarly in the bottom region as well. When k_r is very large, it is also observed that the profiles are approximately symmetric about the middle height ($y = 0.5$), which again illustrates that the effect of the partition becomes negligible. When Ra is increased from 10^4, it is seen that the slopes generally increase, indicating that convection becomes the dominant heat transfer mechanism. For large k_r values, the profiles at the middle of the left half-cavity are almost linear, except at the two end regions, with large slopes which increase when Ra increases. This indicates that a strong and almost linear stratification is well established in the half-cavity. Again the almost symmetric profiles about $y = 0.5$ further show that the effect of the partition becomes negligible when k_r is very large.

The effects of Ra, k_r and T_p can be more evidently demonstrated by the steady-state value of $\theta_{D,y}$, as presented in Fig. 4, where $\theta_{D,y}$ is the temperature difference between the top and bottom of the partition in the middle of the partition (*i.e.*, at $x = 0.5$). It is seen that the steady-state value of $\theta_{D,y}$ increases with increasing Ra when k_r is large (from 10 to 1000). However, when k_r is small ($k_r = 0.1$ and 1), $\theta_{D,}$

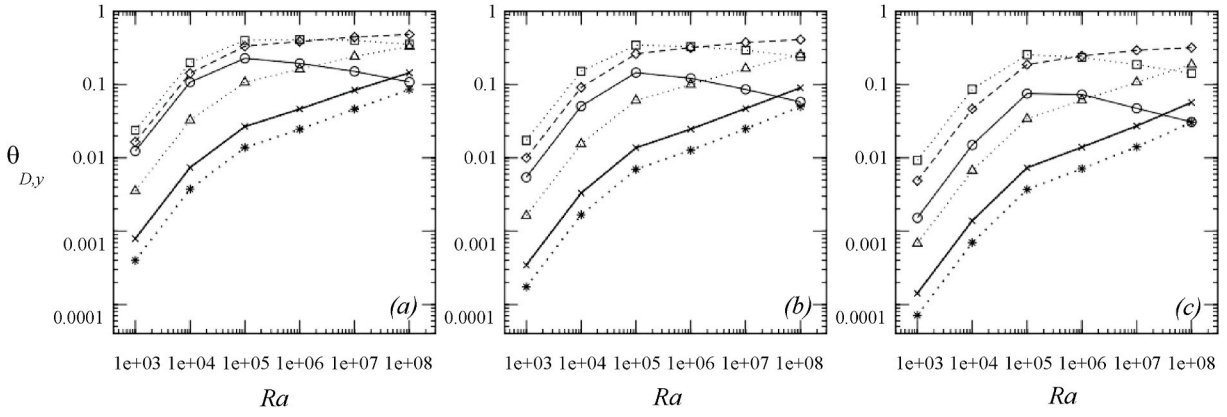

Fig. 4. $\theta_{D,y}$ at $x = 0.5$ at steady state for different Ra, k_r and T_p values: (*a*) $T_p = 0.05$, (*b*) $T_p = 0.1$ and (*c*) $T_p = 0.2$, with $k_r = 0.1$ (solid line), 1 (dotted line), 10 (dashed line), 100 (dotted-dashed line), 500 (bold solid line), and 1000 (bold dotted line).

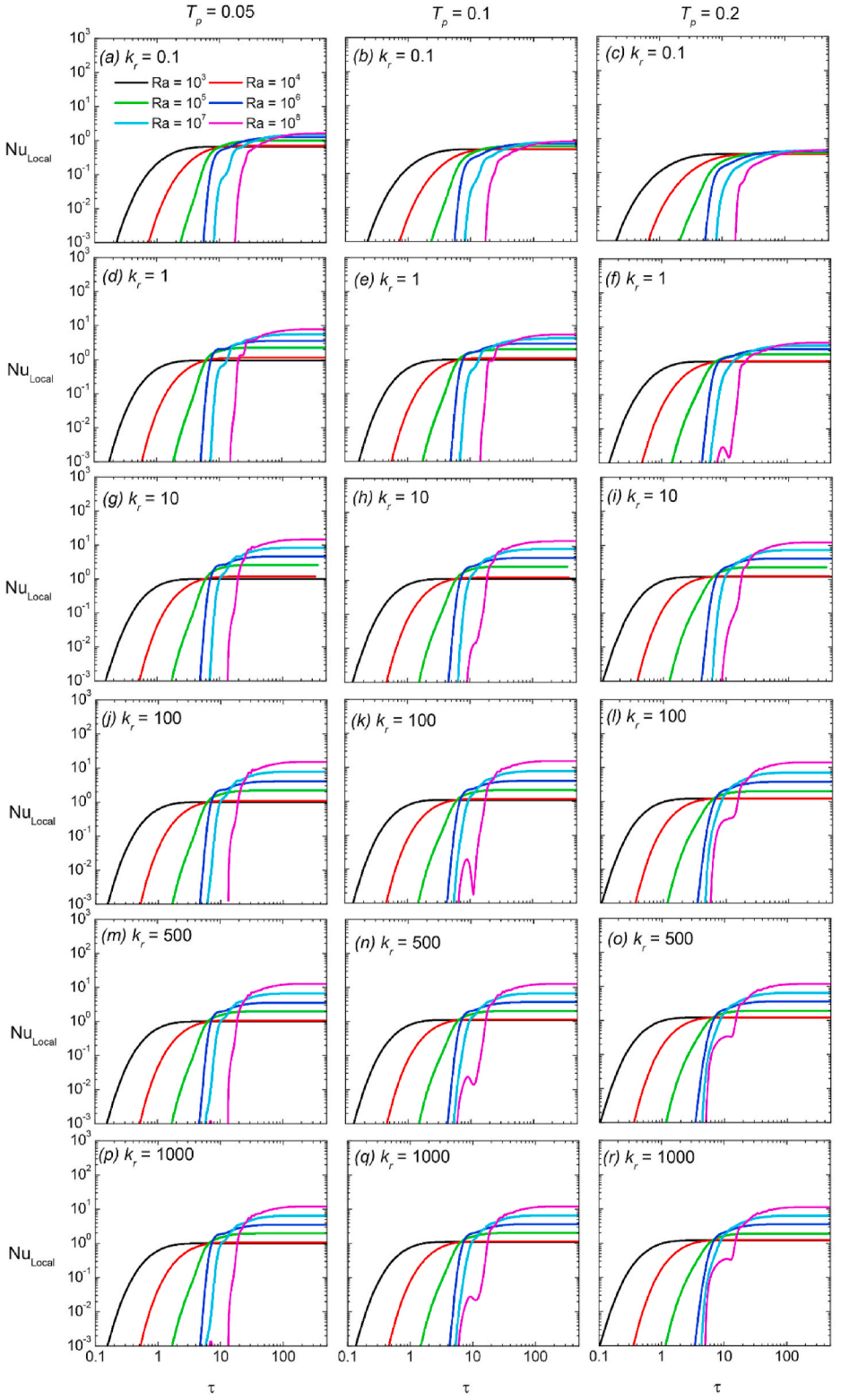

Fig. 5. Time series of $k_r\theta_{D,x}/T_p$ at $y = 0.5$ for different Ra, k_r and T_p values.

$_y$ increases with increasing Ra up to 10^5 only. Beyond that, it decreases when Ra is further increased. The effect of k_r on the steady-state value of $\theta_{D,y}$ is significant, differing significantly for small k_r values and large k_r values. When k_r is large (10 or larger), the increase of k_r substantially reduces $\theta_{D,y}$ for each Ra value. It should be noted that at the steady state, the fluids in either half cavity are well stratified. In the very long run (when the time approaches infinity), the fluid in each half-cavity will become well mixed and approach their respective uniform temperature (1 in the left half-cavity and 0 in the right half-cavity) if the partition is fully insulated ($k_r = 0$), as the flow and heat transfer in each half-cavity are independent each other. On the contrary, if $k_r \to \infty$, from the heat transfer perspective, this partitioned cavity will behave like a non-partitioned cavity without the presence of the partition and it is expected that at the steady state, the fluid in the cavity will become well stratified across the whole width of the cavity, and when time approaches infinity, the fluid in the cavity will become well mixed and approach the uniform temperature of 0.5. This will lead to $\theta_{D,y}$ to drop substantially when k_r increases and approach zero when the time approaches infinity.

3.2. Heat transfer

The main parameter to characterize the transient heat transfer behaviour across the partition is the local Nusselt number, Nu_{local} and the average Nusselt number along the partition, Nu_{ave}. The time series of the local Nusselt number Nu_{local} at the middle height of the partition (*i.e.*, at $y = 0.5$) are presented in Fig. 5 for different Ra, k_r and T_p values. It is seen that for each time series, it takes some time before Nu_{local} to increase monotonically until they become constant when the heat transfer across the partition attains the steady state and the fluid in the cavities is well stratified. The results show that before the steady state Ra has a significance effect on Nu_{local}, as when it increases, the commencement time for Nu_{local} to increase and the time when they attain their respective steady-state values increase substantially.

The effects of Ra, k_r and T_p on the steady-state values of $\theta_{D,x}$ (the temperature difference between the left and the right surfaces of the partition) and Nu_{local} were investigated and the results are shown quantitatively in Fig. S9 in the Supplementary Materials. The results show that when Ra increases from 10^3 to 10^4, both $\theta_{D,x}$ and Nu_{local} essentially do not change. This is apparently due to their conduction-dominant nature. However, when Ra is increased from 10^4 to 10^8, Nu_{local} and $\theta_{D,x}$ increase in the manner of $Nu_{local} = C_1 Ra^n$ and $\theta_{D,x} = C_2 Ra^n$, where C_1, C_2 and n are constants which vary when k_r and T_p change, showing the effects of these parameters on Nu_{local} and $\theta_{D,x}$ at the steady state as well. As $Nu_{local} = (k_r/T_p)\theta_{D,x}$, $C_2 = (T_p/k_r)C_1$. The values of C_1, C_2 and n for each set of k_r and T_p over $10^4 \leq Ra \leq 10^8$ are listed in Table 4. It is apparent that the relations of $Nu_{local} = C_1 Ra^n$ and $\theta_{D,x} = C_2 Ra^n$ are due to the convection-dominant nature when Ra is very large, similar to the relation $Nu_{local} \sim Ra^{1/4}$ for the non-partitioned cavity case [12].

It is seen from Table 4 that both Ra and k_r have significant effects on Nu_{local} and $\theta_{D,x}$. When k_r is very small (*i.e.*, $k_r = 0.1$ considered), the Ra effect is small, with n less than 0.1.

In such cases, the thermal resistance of the partition is high which makes the role played by the partition important and the heat transfer rate is significantly reduced, leading to a larger $\theta_{D,x}$ and a uniform heat flux-like heating condition is dominant along the partition. This behaviour can also be seen in Fig. 2(*a*) as a high density of isotherms, which are almost vertical, in the partition, and the boundary layer thickness along the partition surface is almost like that along a vertical wall with fixed uniform heat flux [24,67], *i.e.*, $\delta_T \sim y^{1/5}$. The wall parameter (*i.e.* $\omega = T_P\, Ra_H^{1/4}/k_r$) suggested by Ref. [31] can also be used to identify this regime as $\omega \sim 1$ for the cases presented in Fig. 5(*a*)–(*c*). Due to the significant role of the partition in the heat transfer when k_r is small, it is expected that T_p strongly influences both Nu_{local} and $\theta_{D,x}$. This is confirmed by the results presented in Table 4, which show that for $k_r = 0.1$, n reduces from 0.09 to 0.06 and to 0.03, while C_2 decreases from 3.3559 to 3.3140 and to 2.6390, when T_p is increased from 0.05 to 0.1 and to 0.2, respectively.

When k_r increases to 1, the Ra effect becomes stronger, with n to be 0.21, 0.17 and 0.13 for $T_p = 0.05$, 0.1 and 0.2, respectively, which also shows the noticeable effect of T_p. A further increase of k_r to 10 leads to even larger n values, *i.e.*, 0.27, 0.27, and 0.25 for $T_p = 0.05$, 0.1 and 0.2, respectively, which shows that the effect of T_p becomes negligible. Nevertheless, any further increase of k_r beyond 10 essentially does not change the values of n, which are close to 1/4 for all T_p values considered, and the values of C_1 vary in a narrow range (between about 0.08 and 0.12), resulting in all quantified correlations of $Nu_{local} = C_1 Ra^n$ almost overlapped each other, as shown in Fig. S9(*d*)–(*f*) in the Supplementary Materials. The results from Ref. [12] show that Nu_{local} across the vertical sidewall, which is the local Nusselt number for the heat transfer from the sidewall to the adjacent fluid in the cavity, at the isothermal condition with a fixed temperature applied on the wall, is proportional to $Ra^{1/4}$. The $n \approx 1/4$ for k_r from 10 to 1000 shown in Table 4 therefore indicates that when k_r is very large, the heat transfer across the partition, where the temperatures on the left and right surfaces of the partition vary, behaves like that across the vertical sidewall at the isothermal condition with a fixed temperature applied on the sidewall [12]. This implies that when k_r is very large, due to the very high thermal conductivity of the partition, the heat transfer from the left half-cavity

Table 4
Regression results showing the effects of Ra, k_r and T_p on Nu_{local} and $\theta_{D,x}/T_p$ over the ranges of $10^4 \leq Ra \leq 10^8$, $0.1 \leq k_r \leq 1000$ and $0.05 \leq T_p \leq 0.2$.

k_r	$T_p = 0.05$			$T_p = 0.1$			$T_p = 0.2$		
	C_1	C_2	n	C_1	C_2	n	C_1	C_2	n
0.1	0.3359	3.3559	0.09	0.3314	3.3140	0.06	0.2639	2.6390	0.03
1	0.1915	0.1915	0.21	0.2557	0.2557	0.17	0.3205	0.3205	0.13
10	0.1067	0.0107	0.27	0.1130	0.0113	0.27	0.1248	0.0125	0.25
100	0.0795	0.0008	0.29	0.0857	0.0009	0.28	0.0957	0.0010	0.27
500	0.0878	0.0002	0.27	0.1016	0.0002	0.26	0.1157	0.0002	0.25
1000	0.0955	0.0001	0.26	0.1081	0.0001	0.26	0.1216	0.0001	0.25

to the right half-cavity across the partition behaves like that without the presence of the partition, although the fluids in the two half-cavities are separated physically by the partition. This is expected, from the heat transfer perspective, as heat on the left surface is quickly transferred to the right surface of the partition at the specific height, acted like there is no solid wall in between. The essentially close to zero values of $\theta_{D,x}$ at very large k_r values, as shown in Fig. S9(*a*)–(*c*) in the Supplementary Materials, further illustrate this behaviour of heat transfer across the partition. The heat transfer within the two half-cavities, although the movement of the fluids are separated by the partition, essentially reduces to that in a single cavity without the partition and thus all results obtained for the single cavity without the partition, as presented in Ref. [12], are applicable here. Due to this, it is expected that T_p does not influence both Nu_{local} and $\theta_{D,x}$ when k_r is very large, which is apparently confirmed by the results presented in Fig. S9 in the Supplementary Materials.

Fig. 6 presents the results for the profiles of Nu_{Local} across the partition at $\tau = 5$, 10, 50, and 680 for different Ra and k_r values, all at $T_p = 0.1$. It is noted that at $\tau = 680$, each case is at its steady state. At $Ra = 10^3$, as shown in Fig. 6(*a*)–(*d*), it is apparent that the heat transfer in both half-cavities is purely due to conduction, illustrated by the uniform distribution of Nu_{local} along the partition for all k_r values and $Nu_{local} = 1$ when $k_r = 1$. For $k_r > 1$, Nu_{local} is slightly larger than 1 due to the heat transfer enhancement caused by higher thermal conductivity of the partition compared to that of the fluid. On the contrary, as expected, Nu_{local} at $k_r = 0.1$ is smaller than 1 due to the heat transfer resistance caused by lower thermal conductivity of the partition. When Ra is increased to 10^4, as shown in Fig. 6(*e*)–

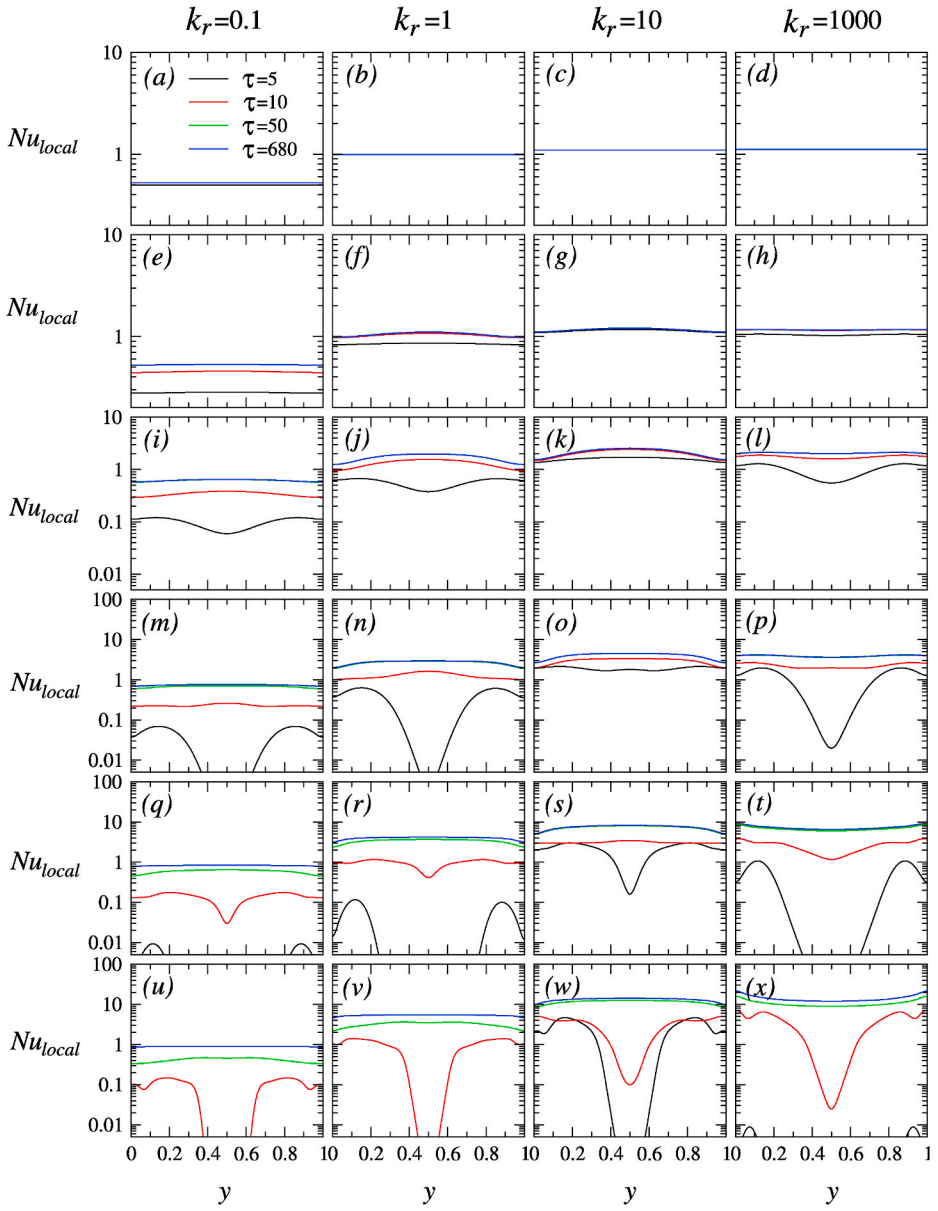

Fig. 6. The profiles of Nu_{Local} across the partition at $\tau = 5$, 10, 50, and 680 for different. Ra and k_r, all at $T_p = 0.1$: (*a*)–(*d*) (first row) $Ra = 10^3$, (*e*)–(*h*) (second row) $Ra = 10^4$, (*i*)–(*l*) (third row) $Ra = 10^5$, (*m*)-(*p*) (fourth row) $Ra = 10^6$, (*q*)-(*t*) (fifth row) $Ra = 10^7$, and (*u*)-(*x*) (sixth row) $Ra = 10^8$.

(*h*), it takes longer for the heat transfer to attain the steady state when compared to $Ra = 10^3$. The values of Nu_{local} are essentially the same as that for $Ra = 10^3$, indicating that the heat transfer in both half-cavities is essentially due to conduction. Nevertheless, the profiles of Nu_{local} on the partition are slightly non-uniform, implying that there is a contribution to the heat transfer from convection, although it is still small. These observations are in agreement with those observed in Section 3.1. With the continuous increase of Ra beyond 10^4, it is seen that convection becomes the dominant heat transfer mechanism, as illustrated by gradually longer times to attain the steady states, stronger non-uniform profiles of Nu_{local} on the partition, and larger values of Nu_{local}. It is also observed that at large k_r

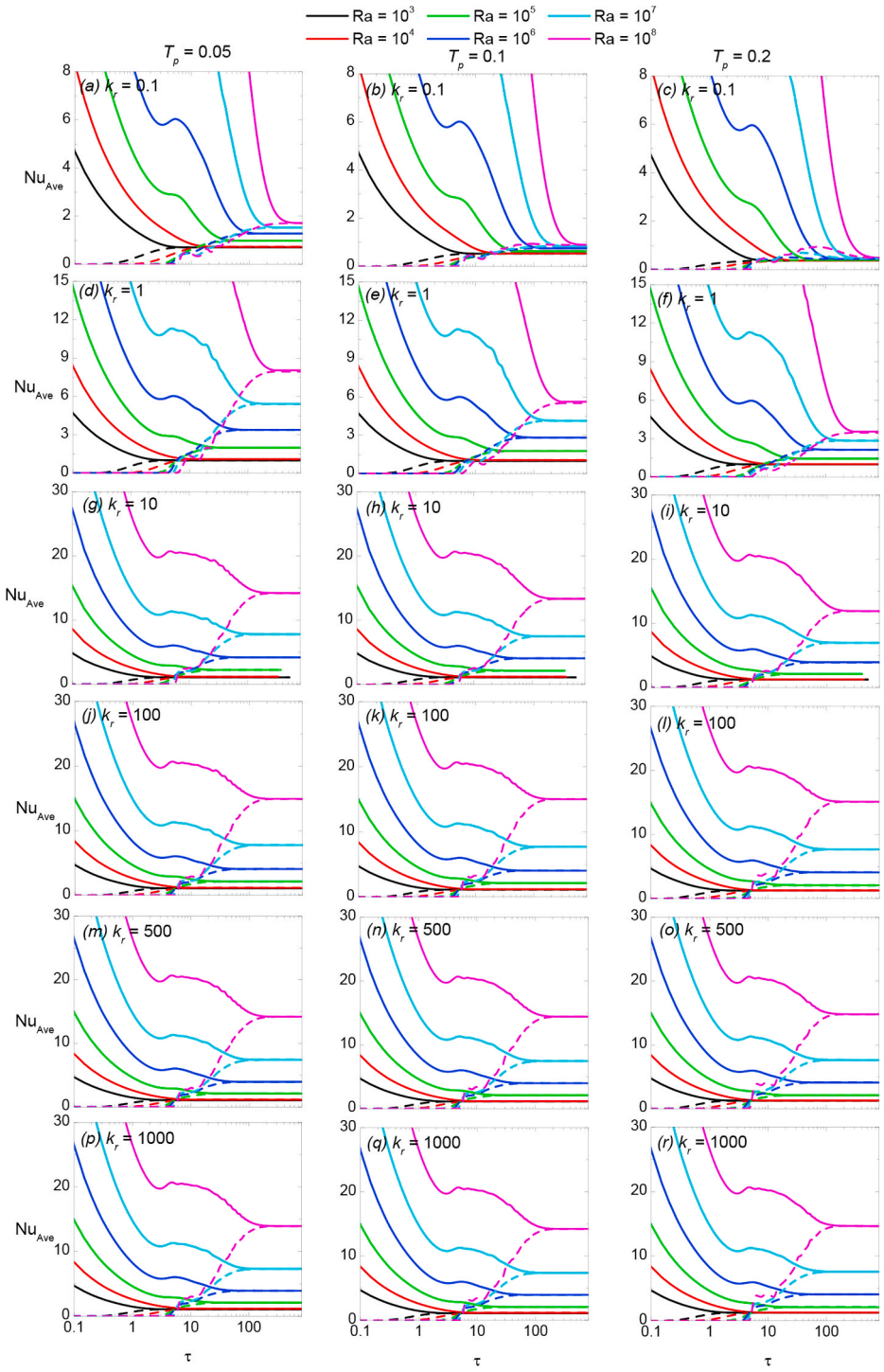

Fig. 7. Time series of Nu_{Ave} on the partition (dashed lines) and the left sidewall (solid lines) for different Ra, k_r and T_p values.

and Ra values, as shown in Fig. 6(t) and (x), the profiles of Nu_{local} are in the form with the values of Nu_{local} decreases slightly from the two ends of the partition toward the middle height where Nu_{local} is the smallest, which is opposite to that at smaller k_r and Ra values. This is due to the thinner boundary layer on the vertical sidewalls which results in thinner intrusions near the top and the bottom regions of the half-cavities and weaker heat transfer by conduction from these regions to the core of the half-cavities.

The development of Nu_{Ave} at the hot sidewall and on the partition experiences four distinct stages, as can be seen in Fig. 7(r) for the case of $Ra = 10^8$, $k_r = 1000$ and $T_p = 0.2$ as an example. At the initial stage, which is very short, the temperature difference between the hot sidewall and the adjacent fluid in the left half-cavity results in the formation of a boundary layer on the sidewall and Nu_{Ave} on the sidewall due to conduction drops quickly. At the same time, as no fluid with a different temperature (other than $\theta = 0.5$) reaches the partition, Nu_{Ave} on the partition is zero. After this conduction stage, the development of the boundary layer on the sidewall is at the quasi steady state, leading to almost constant Nu_{Ave} at the sidewall. During this relatively short stage, the intrusion produced by the boundary layer flow impacts on the partition, which introduces temperature differences at the top and bottom regions of the partition and Nu_{Ave} on the partition increases from zero. When Ra is large, the movements of the boundary layer and the intrusion occur in small regions at the top of the left half-cavity (at the bottom of the right half-cavity as well), leading to heat transfer caused by convection on the partition which is almost constant during this relatively short stage. Subsequently, the continuous movement of the intrusion establishes stratification in the top and bottom regions of both half-cavities, which gradually weakens the heat transfer at the hot sidewall from conduction due to the decreased temperature difference, leading to gradually reduced Nu_{Ave} value. Meanwhile, the temperature differences between the partition surface and the adjacent fluid increase, resulting in the gradually enhanced heat transfer from convection on the partition. This stratification establishment stage, which occurs in a relatively long period, ends when the fluids in both half-cavities are well stratified and the heat transfer at the sidewalls and on the partition attains the steady state, and the value of Nu_{Ave} at the sidewall is equal to that on the partition.

Fig. 7 presents the time series of Nu_{Ave} on the partition and the left sidewall for different Ra, k_r and T_p values. From Fig. 6, it is seen that when τ is not very small (*i.e.*, except the very early stages), the profile of Nu_{local} on the partition is largely uniform. This indicates that the value of Nu_{local} at the middle height of the cavity ($y = 0.5$) well represents the value of Nu_{ave} on the partition, and therefore the characteristics of the transient average heat transfer on the partition Nu_{ave} are essentially the same as those for Nu_{local} at $y = 0.5$ described above for the results presented in Fig. 5. It is therefore that for large k_r values, Nu_{ave} has the same correlation with Ra, that is, $Nu_{ave} = C_3 Ra^n$, where C_3 is another constant. This is confirmed by the results presented in Fig. S10 in the Supplementary Materials, which show that for $Ra \geq 10^4$ all quantified correlations between Nu_{ave} and Ra almost overlap each other. These quantified correlations differ from those for Nu_{local} only by the slight variations of C_3 from C_1 and the values of n are almost identical for Nu_{ave} and Nu_{local} at $y = 0.5$, *i.e.*, $n \approx 1/4$, as presented in Table 5. Hence all discussions and conclusions obtained above for Nu_{local} at $y = 0.5$ are the same for Nu_{ave}.

The time series of $Nu_{ave}/Ra^{1/4}$ against $(1-\tau/\tau_s)^3$ at both the hot sidewall and the partition for different Ra, k_r and T_p values were studied, where τ_s represents the time for the flow in the cavity to attain the steady state, which is determined as the time when the heat transfer in both half-cavities attains the steady state, represented by the instant when Nu_{ave} at the vertical hot sidewall and that on the partition are equal. As shown in Fig. S11 in the Supplementary Materials, it is found that at large Ra values ($Ra > 10^4$) with convection as the dominant flow and heat transfer mechanism, the scaling relation $Nu_{ave}/Ra^{1/4} \sim (1-\tau/\tau_s)^3$, which was obtained by Lin et al. [12] for the non-partitioned case, works well too for the present partitioned cavity, as it brings all time series to overlap each other reasonably well, particularly for large k_r values ($k_r \geq 10$). As discussed above, from the heat transfer perspective, the presence of the partition diminishes quickly when k_r increases beyond 10, reducing the partitioned cavity to the non-partitioned cavity, which makes the scaling relation developed by Lin et al. [12] to be applicable for the present partitioned cavity. However, for small k_r values ($k_r <$ 10), the numerical results deviates noticeably from the scaling relation, further confirming that the heat transfer across the partition behaves like that subjected to a non-isothermal condition applied on a vertical sidewall. It is also noted that at small Ra values ($Ra =$ 10^3 and 10^4) in which the heat transfer is conduction-dominant, the results for the presented partitioned cavity deviates noticeably from the scaling relation for the non-partitioned cavity. This is again in agreement with the observations obtained above.

For the non-partitioned cavity with an isoflux heating condition applied on the vertical sidewall, it was found that $Nu \sim \theta_w Ra^{1/5}$ (see, *e.g.* Refs. [24,68]), where θ_w is the temperature on the wall. For the present partitioned cavity, it is therefore expected that at the partition, $Nu_{Ave} \sim (\theta_{ls} - \theta_{rs}) Ra^{1/5}$, where θ_{ls} and θ_{rs} are temperatures at the left and the right surfaces of the partition, respectively, if the scaling relation $Nu \sim \theta_w Ra^{1/5}$ obtained for the non-partitioned cavity with the iso-flux heating condition is applicable. To examine if this scaling relation is applicable for the presented partitioned cavity, Fig. 8 presents two scaling relations, *i.e.*, $Nu_{Ave} \sim Ra^{1/4}$ and Nu_{Ave} $\sim Ra^{1/5}$ for the lowest k_r value ($k_r = 0.1$). From the results, it is seen that the scaling relation $Nu_{Ave} \sim Ra^{1/5}$ performs better than the scaling relation $Nu_{Ave} \sim Ra^{1/4}$ when Ra is larger, particularly for larger T_p values, indicating that at small k_r values, due to heat

Table 5
Regression results showing the effects of Ra, k_r and T_p on Nu_{Ave} over the ranges of$10^4 \leq Ra \leq 10^8$, $0.1 \leq k_r \leq 1000$ and $0.05 \leq T_p \leq 0.2$.

k_r	$T_p = 0.05$	$T_p = 0.05$	$T_p = 0.1$	$T_p = 0.1$	$T_p = 0.2$	$T_p = 0.2$
	C_3	n	C_3	n	C_3	n
0.1	0.3253	0.09	0.3224	0.06	0.2703	0.03
1	0.1591	0.22	0.2116	0.18	0.2987	0.14
10	0.0947	0.27	0.1032	0.26	0.1261	0.25
100	0.0852	0.28	0.0889	0.28	0.0994	0.27
500	0.0891	0.27	0.0928	0.27	0.1022	0.27
1000	0.0907	0.27	0.0940	0.27	0.1031	0.27

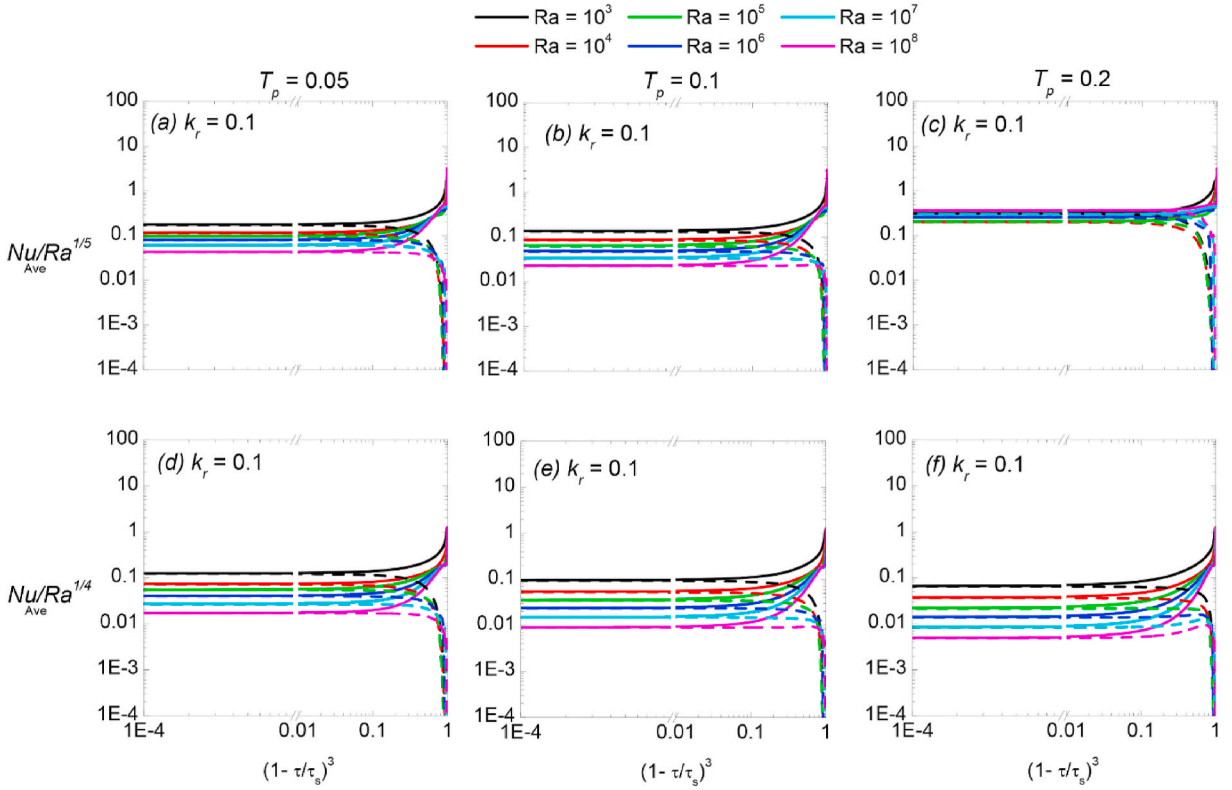

Fig. 8. Time series of $Nu_{Ave}/Ra^{1/4}$ and $Nu_{Ave}/Ra^{1/5}$ on the hot sidewall (solid lines) and the partition (dashed lines) plotted against $(1-(\tau/\tau_s))^3$ for different Ra and T_p values with $k_r = 0.1$.

resistance (which increases when the partition thickness increases), the heat transfer across the partition from convection behaves more like an isoflux heating condition applied on the sidewall, other than the isothermal like heating condition for large k_r values, which is also in agreement with the observation obtained above.

The vertical profiles of $\tau_{o,y}$ at the middle of the left half-cavity for different values of Ra, k_r and T_p, where $\tau_{o,y}$ is denoted as the time for the onset of stratification within the half cavity at the height y and is determined when the absolute value of the temperature difference between that at the point of interest and the initial temperature is greater than 0.01 were investigated. Due to the thick thermal boundary layers for low Ra cases which result in substantial inconsistency in the determination of the values of $\tau_{o,y}$, only the results for $10^6 \leq Ra \leq 10^8$ are studied. The results show that $\tau_{o,y}$ decreases monotonically when y increases, as shown in Fig. S12 in the Supplementary materials. This is expected as the heat transfer mechanisms changes when y increases in the left half-cavity. For large Ra cases, near the top wall region, the heat transfer is mainly due to convection, as the intrusion quickly establishes the stratification of

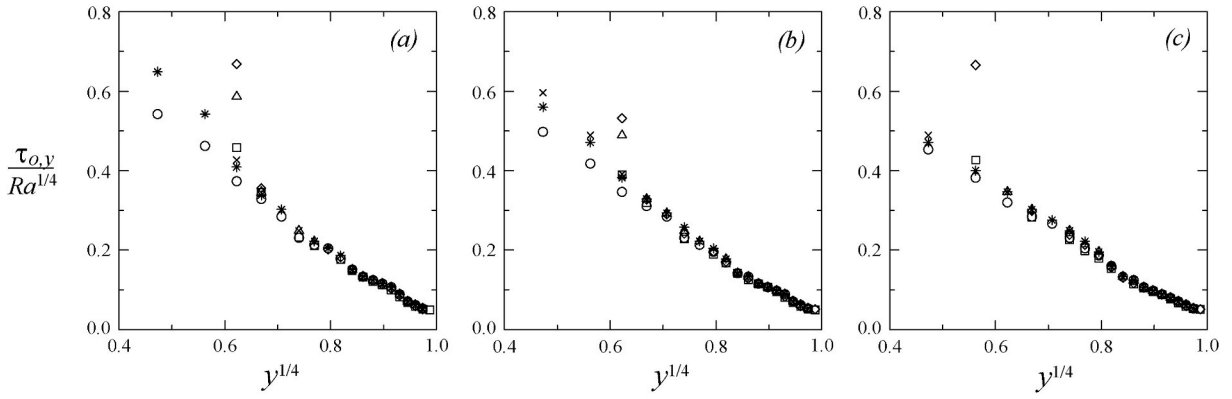

Fig. 9. The vertical profiles of $\tau_{o,y}/Ra^{1/4}$ at the middle of the left half-cavity plotted against $y^{1/4}$ at $Ra = 10^7$ for different k_r and T_p values: (*a*) $T_p = 0.05$, (*b*) $T_p = 0.1$, (*c*) $T_p = 0.2$, with $k_r = 0.1$ (○), 1 (□), 10 (◇), 100 (△), 500 (×), and 1000 (*).

the fluid which results in a very small value of $\tau_{o,y}$. On the contrary, near the bottom wall region, the dominant heat transfer mechanism is due to the horizontal conduction through the partition, which makes the fluid there to take a much longer time to commence the stratification. When y increases from the bottom wall region, the heat transfer mechanisms in the fluid are due to this horizontal conduction through the partition, and additionally, due to the vertical conduction of the fluid at higher heights within the half-cavity from the gradually quicker stratification establishment, resulting in a gradually reduced $\tau_{o,y}$. It is also found that when Ra increases, $\tau_{o,y}$ increases. This is apparently due to the strengthened convective flow which leads to a thinner thermal boundary layer on the vertical sidewall and in turn a thinner intrusion on the top wall, resulting in slower accumulations of the hot fluid in the left half-cavity underneath the top wall and consequently a slower establishment of the stratification.

For large Ra cases, it was shown by Lin et al. [12] and Lin & Armfield [69] that the scaling relation for the boundary layer thickness on the vertical sidewall is $\delta_T \sim y^{1/4}$, which in turn makes the thickness of the intrusion on the top wall scaled by $y^{1/4}$, leading to the establishment of stratification of the fluid in the cavity also to be scaled by $y^{1/4}$, *i.e.*, $\tau_{o,y}/Ra^{1/4} \sim y^{1/4}$. To examine the effects of k_r and T_p on $\tau_{o,y}$, the vertical profiles of $\tau_{o,y}/Ra^{1/4}$ at the middle of the left half-cavity at $Ra = 10^7$ are plotted against $y^{1/4}$ in Fig. 9 for different k_r and T_p. It is observed that in the lower half of the left half-cavity, the effects of k_r and T_p are large and are stronger when y decreases. This is because the stratification establishment in the lower half is mainly due to the horizontal conduction heat transfer through the partition and from the vertically conduction-dominant heat transfer within the fluid, as discussed above, which makes k_r and T_p to play gradually increasing roles in the stratification establishment when y reduces.

However, in the upper half, again as discussed above, the establishment of stratification is mainly caused by convection due to the intrusion near the top region, which makes the contribution to the heat transfer from the horizontal conduction through the partition much smaller, and therefore the influence from k_r is much weaker. This results in the overlap of the scaled profiles of $\tau_{o,y}/Ra^{1/4} \sim y^{1/4}$ for the majority of the upper half of the left half-cavity, particularly near the top region when the effect of k_r is negligible. As the partition thickness increases, $\tau_{o,y}$ drops, which is apparently mainly caused by the reduction of the size of the half-cavity that accelerates the thermal stratification process.

4. Conclusion

The results in this study show that the transient behaviour of the conjugate natural convection flow and heat transfer in the partitioned cavity is mainly governed by Ra. k_r can have a significant effect when it is in the range of 0.1–10 for the values considered, when the role played by the partition changes from resistance to the heat transfer to enhance the heat transfer from one half-cavity to the other through the partition. However, its effect becomes negligible when it is very large, which leads to the transient behaviour of heat transfer in the partitioned cavity to be basically the same as that in the non-partitioned cavity and the scaling relations developed for the non-partitioned cavity is found to be generally applicable for the partitioned cavity. The effect of T_p on heat transfer is significant mainly when k_r is small (less than 10). In addition, it speeds up the stratification establishment in the half-cavity when it increases, due to the resulted reduction of the size of the half-cavity. The results also show that although the natural convection boundary layers and heat transfer on the vertical sidewalls of the cavity are produced by an isothermal condition, the presence of the partition with various thermal conductivity, makes the partition to behave like an isoflux wall for small k_r values ($k_r \leq 1$), and like an isothermal wall for large k_r values ($k_r \geq 10$).

CRediT authorship contribution statement

Mehdi Khatamifar: Conceptualization, Methodology, Investigation, Writing – original draft. **Wenxian Lin:** Supervision, Conceptualization, Writing – review & editing. **Liqiang Dong:** Methodology.

Declaration of competing interest

The authors declare that they have no known competing financial interests or personal relationships that could have appeared to influence the work reported in this paper.

Acknowledgment

The support from the Australian Research Council (Discovery Project grant DP130100900) is gratefully acknowledged.

Appendix A. Supplementary data

Supplementary data to this article can be found online at https://doi.org/10.1016/j.csite.2021.100952.

References

[1] M. Khatamifar, W. Lin, S.W. Armfield, D. Holmes, M.P. Kirkpatrick, Conjugate natural convection heat transfer in a partitioned differentially-heated square cavity, Int. Commun. Heat Mass Tran. 81 (2017) 92–103.

[2] H.P. Rani, C.N. Kim, Transient convection on a vertical cylinder with variable viscosity and thermal conductivity, J. Thermophys. Heat Tran. 22 (2) (2008) 254–261.
[3] I. Pop, D.B. Ingham, P. Cheng, Transient free convection between two concen- tric spheres filled witha porous medium, J. Thermophys. Heat Tran. 7 (4) (1993) 724–727.
[4] D. Li, Z. Yu, Natural convection melting in a cubic cavity with internal fins: a lattice Boltzmann study methods have been proposed to enhance the heat, Case Studies in Thermal Engineering (2021), https://doi.org/10.1016/j.csite.2021.100919. In press.
[5] M.A. Kumar, Y.D. Reddy, V.S. Rao, B.S. Goud, Thermal radiation impact on mhd heat transfer natural convective nano fluid flow over an impulsively started vertical plate, Case Studies in Thermal Engineering 24 (2021) 100826.
[6] D. Xu, Y. Hu, D. Li, A lattice Boltzmann investigation of two-phase natural convection of cu-water nanofluid in a square cavity, Case Studies in Thermal Engineering 13 (2019) 100358.
[7] S.E. Ahmed, Z.Z. Rashed, Mhd natural convection in a heat generating porous medium- filled wavy enclosures using buongiorno's nanofluid model, Case Studies in Thermal Engi- neering 14 (2019) 100430.
[8] M. Akbarzadeh, S. Rashidi, N. Karimi, R. Ellahi, Convection of heat and thermody- namic irreversibilities in two-phase,turbulent nanofluid flows in solar heaters by corrugated absorber plates, Adv. Powder Technol. 29 (2018) 2243–2254.
[9] R. Ellahi, A. Zeeshan, N. Shehzad, S.Z. Alamri, Structural impact of kerosene- Al2O3 nanoliquid on MHD Poiseuille flow with variable thermal conductivity: application of cooling process, J. Mol. Liq. 264 (2018) 607–615.
[10] A.A. Khan, S. Naeem, R. Ellahi, S.M. Sait, K. Vafai, Dufour and soret effects on Darcy-forchheimer flow of second-grade fluid with the variable magnetic field and ther- mal conductivity, Int. J. Numer. Methods Heat Fluid Flow 30 (9) (2020) 4331–4347.
[11] J.C. Patterson, S.W. Armfield, Transient features of natural convection in a cavity, J. Fluid Mech. 219 (1990) 469–497.
[12] W. Lin, S.W. Armfield, J.C. Patterson, Cooling of a Pr < 1 fluid in a rectangular container, J. Fluid Mech. 574 (2007) 85–108.
[13] M.N. Hasan, S.C. Saha, Y.T. Gu, Unsteady natural convection within a differentially heated enclosure of sinusoidal corrugated side walls, Int. J. Heat Mass Tran. 55 (2012) 5696–5708.
[14] Q. Wang, W. Li, Z. Chen, D.J. Kukulka, Numerical analysis on natural convection in various enclosures, Numer. Heat Tran., Part A: Applications 77 (4) (2020) 391–408.
[15] Y. Billaud, D. Saury, D. Lemonnier, Numerical investigation of coupled natural con- vection and radiation in a differentially heated cubic cavity filled with humid air. Effects of the cavity size, Numer. Heat Tran., Part A: Applications 72 (7) (2017) 495–518.
[16] W. Lin, S.W. Armfield, J.C. Patterson, Unsteady natural convection boundary-layer flow of a linearly-stratified fluid with Pr < 1 on an evenly heated semi-infinite vertical plate, Int. J. Heat Mass Tran. 51 (2008) 327–343.
[17] S.C. Saha, R.J. Brown, Y.T. Gu, Prandtl number scaling of the unsteady natural convection boundary layer adjacent to a vertical flat plate for Pr > 1 subject to ramp surface heat flux, Int. J. Heat Mass Tran. 55 (23–24) (2012) 7046–7055.
[18] W. Lin, S.W. Armfield, Scalings for unsteady natural convection boundary layers on a vertical plate at time-dependent temperature, Int. J. Therm. Sci. 111 (2017) 78–99.
[19] W. Lin, S.W. Armfield, Natural convection boundary-layer flow on an evenly heated vertical plate with time-varying heating flux in a stratified Pr < 1 fluid, Numer. Heat Tran., Part A: Applications 76 (6) (2019) 393–419.
[20] L. Zhou, S.W. Armfield, N. Williamson, M. Kirkpatrick, W. Lin, Natural convection in a cavity with time-varying thermal forcing on a sidewall, Int. J. Heat Mass Tran. 150 (2020), 119234.
[21] J.C. Patterson, J. Imberger, Unsteady natural convection in a rectangular cavity, J. Fluid Mech. 100 (1980) 65–86.
[22] F. Xu, J.C. Patterson, C. Lei, Heat transfer through coupled thermal boundary layers induced by a suddenly generated temperature difference, Int. J. Heat Mass Tran. 52 (2009) 4966–4975.
[23] S.C. Saha, R.J. Brown, Y.T. Gu, Scaling for the Prandtl number of the natu- ral convection boundary layer of an inclined flat plate under uniform surface heat flux, Int. J. Heat Mass Tran. 55 (2012) 2394–2401.
[24] W. Lin, S.W. Armfield, Scalings for unsteady natural convection boundary layers on an evenly heated plate with time-dependent heating flux, Phys. Rev. 88 (2013), 063013.
[25] M.A. Antar, H. Baig, Conjugate conduction-natural convection heat transfer in a hollow building block, Appl. Therm. Eng. 29 (17–18) (2009) 3716–3720.
[26] A. Liaqat, A.C. Baytas, Numerical comparison of conjugate and non-conjugate natural convection for internally heated semi-circular pools, Int. J. Heat Fluid Flow 22 (6) (2001) 650–656.
[27] F. Xu, Unsteady coupled thermal boundary layers induced by a fin on the partition of a differentially heated cavity, Int. Commun. Heat Mass Tran. 67 (2015) 59–65.
[28] N. Williamson, S.W. Armfield, M.P. Kirkpatrick, Transition to oscillatory flow in a differentially heated cavity with a conducting partition, J. Fluid Mech. 693 (2012) 93–114.
[29] R. Viskanta, M. Abrams, Thermal interaction of two streams in boundary-layer flow separated by a plate, Int. J. Heat Mass Tran. 14 (9) (1971) 1311–1321.
[30] G.S.H. Lock, R.S. Ko, Coupling through a wall between two free convective systems, Int. J. Heat Mass Tran. 16 (1973) 2087–2096.
[31] R. Anderson, A. Bejan, Natural convection on both sides of a vertical wall separating fluids at different temperatures, J. Heat Tran. 102 (1980) 631–635.
[32] A. Bejan, R. Anderson, Heat transfer across a vertical impermeable partition imbedded in porous medium, Int. J. Heat Mass Tran. 24 (7) (1981) 1237–1245.
[33] P.K. Ghosh, A. Sarkar, V.M.K. Sastri, Natural convection heat transfer in an enclosure with a partition-a finite-element analysis, Numer. Heat Tran. 21 (1992) 231–248.
[34] T.W. Tong, F.M. Gerner, Natural convection in partitioned air-filled rectangular enclosures, Int. Commun. Heat Mass Tran. 13 (1986) 99–108.
[35] K. Kahveci, Numerical simulation of natural convection in a partitioned enclosure us- ing PDQ method, Int. J. Numer. Methods Heat Fluid Flow 17 (2007) 439–456.
[36] A. Kangni, R.B. Yedder, E. Bilgen, Natural convection and conduction in enclo- sures with multiple vertical partitions, Int. J. Heat Mass Tran. 34 (1991) 2819–2825.
[37] K. Kahveci, A differential quadrature solution of natural convection in an enclosure with a finite-thickness partition, Numer. Heat Tran., Part A: Applications 51 (2007) 979–1002.
[38] D. Duxbury, An Interferometric Study of Natural Convection in Enclosed Plane Air Layers with Complete and Partial Central Vertical Divisions, PhD thesis, University of Salford, 1979.
[39] T. Nishimura, M. Shiraishi, F. Nagasawa, Y. Kawamura, Natural convection heat transfer in enclosures with multiple vertical partitions, Int. J. Heat Mass Tran. 31 (1988) 1679–1686.
[40] D.M. Cuckovic-Dzodzo, M.B. Dzodzo, M.D. Pavlovic, Laminar natural convection in a fully partitioned enclosure containing fluid with nonlinear thermophysical properties, Int. J. Heat Fluid Flow 20 (6) (1999) 614–623.
[41] R. Anderson, A. Bejan, Heat transfer through single and double vertical walls in natural convection: theory and experiment, Int. J. Heat Mass Tran. 24 (1981) 1611–1620.
[42] N. Williamson, S.W. Armfield, Stability characteristics of conjugate natural convection boundary layers, ANZIAM J. 52 (2011) 696–709.
[43] S. Saha, S. Barua, B. Kushwaha, S. Subedi, M.N. Hasan, S.C. Saha, Conjugate natural convection in a corrugated solid partitioned differentially heated square cavity, Numer. Heat Tran., Part A: Applications 78 (10) (2020) 541–559.
[44] S. Acharya, C.H. Tsang, Natural convection in a fully partitioned, inclined enclosure, Numer. Heat Tran. 8 (1985) 407–428.
[45] H. Turkoglu, N. Yücel, Natural convection heat transfer in enclosures with conducting multiple partitions and side walls, Heat and Mass Transfer/Waerme- und Stoffuebertragung 32 (1–8) (1996).
[46] K. Hanjalić, S. Kenjereš, F. Durst, Natural convection in partitioned two-dimensional enclosures at higher Rayleigh numbers, Int. J. Heat Mass Tran. 39 (1996) 1407–1427.

[47] M.W. Nansteel, R. Greif, Natural convection in undivided and partially divided rect- angular enclosures, J. Heat Tran. 103 (1981) 623–629.
[48] F. Xu, Q. Yang, P. Yu, Numerical studies of transition from steady to unsteady coupled thermal boundary layers, Int. J. Comput. Methods 11 (2014) 1344002.
[49] H. Wang, C. Lei, A numerical investigation of conjugate thermal boundary layers in a differentially heated partitioned cavity filled with different fluids, Phys. Fluids 32 (2020), 074107.
[50] S.C. Saha, M.M.K. Khan, Y.T. Gu, Unsteady buoyancy driven flows and heat transfer through coupled thermal boundary layers in a partitioned triangular enclosure, Int. J. Heat Mass Tran. 68 (2014) 375–382.
[51] C. Wan, B.S.V. Patnaik, D.G.W. Wei, A new benchmark quality solution for the buoyancy-driven cavity by discrete singular convolution, Numer. Heat Tran. Part B: Fundamentals 40 (2001) 199–228.
[52] W.H. Leong, K.G.T. Hollands, A.P. Brunger, Experimental nusselt numbers for a cubical-cavity benchmark problem in natural convection, Int. J. Heat Mass Tran. 42 (1999) 1979–1989.
[53] Y.J. Choi, *A Numerical Study on a Lumped-Parameter Model and a CFD Code Coupling for the Analysis of the Loss of Coolant Accident in a Reactor Containment*. PhD Thesis, Université de Marne-la-Vallée, 2005.
[54] D.R. Chenoweth, S. Paolucci, Natural convection in an enclosed vertical air layer with large horizontal temperature differences, J. Fluid Mech. 169 (1986) 173–210.
[55] H.N. Dixit, V. Babu, Simulation of high Rayleigh number natural convection in a square cavity using the lattice Boltzmann method, Int. J. Heat Mass Tran. 49 (2006) 727–739.
[56] K. Khanafer, K. Vafai, M. Lightstone, Buoyancy-driven heat transfer enhancement in a two-dimensional enclosure utilizing nanofluids, Int. J. Heat Mass Tran. 46 (2003) 3639–3653.
[57] G. De Vahl Davis, Natural convection of air in a square cavity: a bench mark numerical solution, Int. J. Numer. Methods Fluid. 3 (1983) 249–264.
[58] P. Le Quéré, T.A. De Roquefortt, Computation of natural convection in two- dimensional cavities with Chebyshev polynomials, J. Comput. Phys. 57 (1985) 210–228.
[59] P. Le Quéré, Accurate solutions to the square thermally driven cavity at high Rayleigh number, Comput. Fluid 20 (1991) 29–41.
[60] R. Puragliesi, Numerical Investigation of Particle-Laden Thermally Driven Turbulent Flows in Enclosure, PhD thesis, École Polytechnique Fédérale De Lausanne, 2010.
[61] S.F. Corzo, S.M. Damián, D. Ramajo, N.M. Nigro, Numerical simulation of natural convection phenomena, Mecánica Computacional 30 (2011) 277–296.
[62] M.T. Manzari, An explicit finite element algorithm for convection heat transfer problems, Int. J. Numer. Methods Heat Fluid Flow 9 (1999) 860–877.
[63] R.S. Graves, R.R. Zarr, Insulation Materials, Testing and Applications, in: 3rd Volume, ASTM Special Technical Publication. American Society for Testing Materials, 1997.
[64] L.L.C. Aerogel Technologies, Silica Aerogel, 1999.
[65] W. Lin, S.W. Armfield, Natural convection cooling of rectangular and cylindrical containers, Int. J. Heat Fluid Flow 22 (2001) 72–81.
[66] W. Lin, S.W. Armfield, Long-term behavior of cooling fluid in a rectangular container, Phys. Rev. 69 (2004), 056315.
[67] A. Bejan, Convection Heat Transfer, fourth ed., John Wiley & Sons, 2013.
[68] S.W. Armfield, J.C. Patterson, W. Lin, Scaling investigation of the natural convection boundary layer on an evenly heated plate, Int. J. Heat Mass Tran. 50 (7–8) (2007) 1592–1602.
[69] W. Lin, S.W. Armfield, Unified Prandtl number scaling for start-up and fully developed natural-convection boundary layers for both $Pr \gtrsim 1$ and $Pr \lesssim 1$ fluids with isothermal heating, Phys. Rev. 86 (2012), 066312.